Monthly Notices
of the
ROYAL ASTRONOMICAL SOCIETY

MNRAS **454,** 839–848 (2015) doi:10.1093/mnras/stv2054

The VMC survey – XVI. Spatial variation of the cluster formation activity in the innermost regions of the Large Magellanic Cloud

Andrés E. Piatti,[1,2]★ Richard de Grijs,[3,4,5] Vincenzo Ripepi,[6] Valentin D. Ivanov,[7] Maria-Rosa L. Cioni,[8,9,10] Marcella Marconi,[6] Stefano Rubele,[11] Kenji Bekki[12] and Bi-Qing For[12]

[1]*Observatorio Astronómico, Universidad Nacional de Córdoba, Laprida 854, 5000 Córdoba, Argentina*
[2]*Consejo Nacional de Investigaciones Científicas y Técnicas, Av. Rivadavia 1917, C1033AAJ Buenos Aires, Argentina*
[3]*Kavli Institute for Astronomy and Astrophysics, Peking University, Yi He Yuan Lu 5, Hai Dian District, Beijing 100871, China*
[4]*Department of Astronomy, Peking University, Yi He Yuan Lu 5, Hai Dian District, Beijing 100871, China*
[5]*International Space Science Institute–Beijing, 1 Nanertiao, Zhongguancun, Hai Dian District, Beijing 100190, China*
[6]*INAF, Osservatorio Astronomico di Capodimonte, via Moiariello 16, I-80131 Napoli, Italy*
[7]*European Southern Observatory, Karl-Schwarzschild-Strasse 2, D-85748 Garching bei Munchen, Germany*
[8]*Institut für Physik und Astronomie, Universität Potsdam, Karl-Liebknecht-Str. 24/25, D-14476 Potsdam, Germany*
[9]*Leibnitz-Institut für Astrophysik Potsdam, An der Sternwarte 16, D-14482 Potsdam, Germany*
[10]*Physics Astronomy and Mathematics, University of Hertfordshire, College Lane, Hatfield AL10 9AB, UK*
[11]*INAF, Osservatorio Astronomico di Padova, vicolo dell'Osservatorio 5, I-35122 Padova, Italy*
[12]*ICRAR, University of Western Australia, 35 Stirling Hwy, Crawley WA 6009, Australia*

Accepted 2015 September 2. Received 2015 September 2; in original form 2015 July 27

ABSTRACT

We present results based on YJK_s photometry of star clusters in the Large Magellanic Cloud (LMC), distributed throughout the central part of the galaxy's bar and the 30 Doradus region. We analysed the field-star-decontaminated colour–magnitude diagrams of 313 clusters to estimate their reddening values and ages. The clusters are affected by a mean reddening of $E(B-V) \in [0.2, 0.3]$ mag, where the average internal LMC reddening amounts to ∼0.1–0.2 mag. The region covering 30 Doradus includes clusters with reddening values in excess of $E(B-V) = 0.4$ mag. Our cluster sample spans the age range $7.0 \leq \log(t\ \mathrm{yr}^{-1}) < 9.0$, represents an increase of 30 per cent in terms of the number of clusters with robust age estimates and comprises a statistically complete sample in the LMC regions of interest here. The resulting cluster frequencies suggest that the outermost regions of the LMC bar first experienced enhanced cluster formation – $\log(t\ \mathrm{yr}^{-1}) \in [8.5, 9.0]$ – before the activity proceeded, although in a patchy manner, to the innermost regions, for $\log(t\ \mathrm{yr}^{-1}) < 7.7$. Cluster frequencies in the 30 Doradus region show that the area is dominated by very recent cluster formation. The derived star formation frequencies suggest that the cluster and field-star populations do not seem to have fully evolved as fully coupled systems during the last ∼100 Myr.

Key words: techniques: photometric – galaxies: individual: LMC – Magellanic Clouds.

1 INTRODUCTION

The galaxies in the Local Group are uniquely suitable to verify the results of analyses based on integrated cluster properties using resolved stellar photometry (e.g. de Grijs & Anders 2006; Colucci & Bernstein 2012; Baumgardt et al. 2013; Cezario et al. 2013; de Meulenaer et al. 2013). Dedicated photometric surveys of the Magellanic Clouds at both optical and near-infrared wavelengths are now probing sufficiently deeply so that we have a reasonable chance at resolving individual stars to well below the main-sequence turn-off (MSTO) magnitudes characteristic of old stellar populations. With our unparalleled access to deep near-infrared observations obtained with the 4-m Visible and Infrared Survey Telescope for Astronomy (VISTA; Emerson, McPherson & Sutherland 2006; Emerson & Sutherland 2010) as part of the VISTA near-infrared Y, J, K_s survey of the Magellanic System (VMC) the star cluster systems in the Small and Large Magellanic Clouds (SMC, LMC) can now be studied in detail to provide unique insights into the properties of their resolved star cluster populations.

★ E-mail: andres@oac.uncor.edu

© 2015 The Authors
Published by Oxford University Press on behalf of the Royal Astronomical Society

Downloaded from https://academic.oup.com/mnras/article-abstract/454/1/839/1143215 by guest on 24 April 2020

In this paper, we address a long-standing issue of contention in Magellanic Clouds studies, i.e. that of the coupling (if any) between field-star and (massive) star cluster formation (i.e. for cluster masses $M_{\rm cl} \gtrsim 10^4$ M$_\odot$). The LMC exhibits a well-known gap in the (massive) cluster age distribution between ∼3 and 13 Gyr, while the age distribution of the field stellar population appears more continuous. Numerous authors have asserted that the LMC's field-star and star cluster formation histories are significantly different (e.g. Olszewski, Suntzeff & Mateo 1996; Geha et al. 1998; Sarajedini 1998, and references therein). The situation for the SMC is less straightforward, although Rafelski & Zaritsky (2005) provide tentative evidence that the cluster and field-star age distributions may also be significantly different in this system (see also Gieles, Lamers & Portegies Zwart 2007). Similarly, the observed disparities between the cluster and field-star age distributions in the (dwarf) starburst galaxies NGC 1569 (Anders et al. 2004) and M82 (Barker, de Grijs & Cerviño 2008) seem to offer evidence in support of a decoupling between star cluster and field-star formation. If confirmed, this would be consistent with the view that massive star cluster formation requires special conditions, e.g. large-scale gas flows, in addition to the presence of dense gas (cf. Ashman & Zepf 1992; Elmegreen & Efremov 1997; de Grijs, O'Connell & Gallagher 2001). However, this scenario may well only apply to the most massive star clusters, whereas lower mass clusters could indeed be following the field-star formation history more closely. This is our main scientific driver here.

This is indeed an issue of general interest in the field of star and star cluster formation, given the commonly held notion that 70–90 per cent of stars with masses in excess of 0.5 M$_\odot$ may form in clustered environments (e.g. Lada & Lada 2003). Since most present-day stars in galaxies like the Milky Way and the Magellanic Clouds form part of their host galaxies' field stellar population, it is not a stretch to suggest that a significant fraction of those field stellar populations originate from disrupted clusters, whether or not the latter were in fact gravitationally bound to begin with.

There is now significant evidence that star cluster systems appear to be affected by a disruption mechanism that acts on very short time-scales ($\lesssim$10–30 Myr) and which may be mass independent, at least for masses $\gtrsim 10^4$ M$_\odot$ (e.g. Bastian et al. 2005; Fall, Chandar & Whitmore 2005; Fall 2006). This fast disruption mechanism, which is thought to disrupt up to 50–90 per cent of the youngest clusters in a given cluster population (e.g. Lada & Lada 1991; Whitmore 2004; Bastian et al. 2005; Mengel et al. 2005; Goodwin & Bastian 2006; Whitmore, Chandar & Fall 2007), is in essence caused by the rapid removal of the intracluster gas on time-scales of $\lesssim$30 Myr, a process coined cluster 'infant mortality' (Lada & Lada 2003); it was originally reported in the context of the number of very young embedded clusters in the Milky Way, compared to their older, largely gas-free counterparts.

Those clusters that survive the infant mortality phase will be subject to the processes driving longer term star cluster dissolution (see for reviews de Grijs & Parmentier 2007; de Grijs 2010). The longer term dynamical evolution of star clusters is determined by a combination of internal and external time-scales. These processes depend on the actual cluster masses, with more massive clusters being more resilient to disruptive influences. Based on these arguments, one would expect that the lower mass clusters in a given cluster population are the dominant donors of stars to their host galaxies' field-star populations, while the higher mass cluster formation and evolution history is not directly coupled to the field-star properties. In the context of the LMC's star cluster population, cluster disruption has been the subject of much debate. Nevertheless, and despite having access to cluster samples exceeding 900 members, the jury is still out as regards the typical time-scale of cluster disruption (e.g. Parmentier & de Grijs 2008) and whether this may vary as a function of position in the galaxy (e.g. Bagheri, Cioni & Napiwotzki 2013; de Grijs, Goodwin & Anders 2013, and references therein).

This paper is organized as follows. Section 2 provides an overview of the data on which this study is based and the data reduction procedures applied. We define our statistically complete LMC cluster sample in Section 3, and use isochrone fits to determine the clusters' best-fitting physical parameters in Section 4. Section 5 addresses the key questions posed in this study; in particular, we consider the cluster frequencies (CFs) across the LMC and compare the cluster formation rates with the star formation rates (SFRs) in the corresponding field regions. We present our main conclusions in Section 6.

2 DATA HANDLING

The VMC and its initial data are thoroughly described in Cioni et al. (2011), to which we refer the reader for details. Here, we used data of two VMC tiles located in the central part of the LMC bar (LMC 6_4) and in a region covering the 30 Doradus star-forming region (LMC 6_6), for which the VISTA imaging campaign has been completed. These regions are of significant scientific interest, since they contain a large number of star clusters which can provide statistical results about the central region of the LMC where other tiles are still being observed. Indeed, the purpose of this paper is to present a photometric analysis of the catalogued clusters located in those regions based on the most complete VMC data set to date. The available photometric data allow us to confirm the physical reality of the catalogued star clusters and estimate their fundamental parameters. We also investigate the CF in the regions of interest to assess whether star clusters and field stars have evolved as a coupled system. Fig. 1 shows the location of all LMC tiles of the VMC survey. The red rectangles mark those used in this paper.

The tile LMC 6_4 and 6_6 data refers to observations acquired from 2010 October until 2011 November and from 2009 November to 2010 October, respectively. Seeing constraints, imposed for the purpose of homogenizing crowded and uncrowded field observations, range between 1.0 and 1.3 arcsec (Y), 0.9 and 1.2 arcsec (J), and 0.8 and 1.0 arcsec ($K_{\rm s}$) and may exceed those values by 10 per cent according to observing policy. One tile covers uniformly an area of ∼1.5 deg^2, as a result of the mosaic of six paw-print images, in a given waveband with 3 epochs at Y and J, and 12 epochs at $K_{\rm s}$. Individual epochs have exposure times of 800 s (Y and J) and 750 s ($K_{\rm s}$). We used the v1.3 VMC release paw-prints. They were processed by the VISTA Data Flow System's (VDFS; Emerson et al. 2004) pipeline (Irwin et al. 2004) and retrieved from the VISTA Science Archive (VSA; Hambly et al. 2004). The processed paw-print images were used to derive the effective point spread functions (PSFs) using the IRAF/DAOPHOT routines (Stetson, Davis & Crabtree 1990). We generated a reference PSF, which was convolved with the paw-print images to homogenize the resulting PSFs. We repeated these steps for each epoch separately. Finally, all homogenized paw-print images were combined using the SWARP tool (Bertin et al. 2002), as described in Rubele et al. (2012), thus generating deep tile images with homogeneous PSFs.

We performed PSF photometry using the IRAF/DAOPHOT package to generate photometric catalogues which return right ascension and declination, object magnitude, its error and sharpness, local magnitude completeness, and number of stars used to compute the latter in the Y, J, $K_{\rm s}$ passbands for ∼2.6 million of sources in each

Downloaded from https://academic.oup.com/mnras/article-abstract/454/1/839/1143215 by guest on 24 April 2020

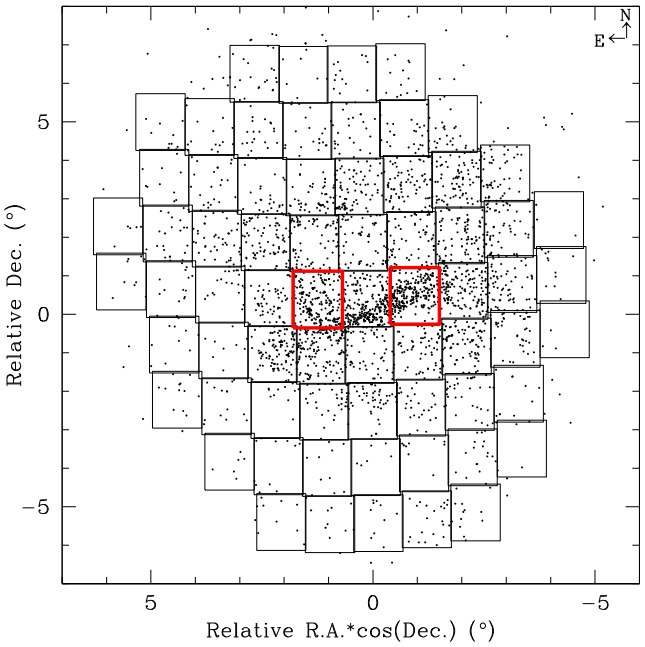


Figure 1. Spatial distribution of the Bica et al. (2008) catalogue of star clusters in the LMC centred at RA = $05^{h}23^{m}34^{s}$, Dec. = $-69°45'22''$ (J2000), projected on to the sky. The objects studied in this paper are located in tiles highlighted as red rectangles: LMC 6_4 (right) and LMC 6_6 (left). The remaining VMC tiles across the LMC are shown as black rectangles.

tile. We used the PSF task to produce the PSF model (which varies across the sky) and the ALLSTAR task to perform our photometry, using a radius of three pixels. We checked that our PSF photometry produced results consistent with those provided by the VSA for the bulk of the observed stars (Rubele et al. 2012, 2015). The final photometric catalogues are publicly available both at the VSA[1] and ESO[2] science archives.

We ran a large number of artificial-star tests to estimate the incompleteness and error distribution of our photometric catalogues for each tile and in every part of the colour–magnitude diagram (CMD), as described in Rubele et al. (2012), where the photometry for two small subregions in tile LMC 6_6 is presented. Photometric errors of 0.10 mag were derived for stars with $Y = 20.8$ mag, $J = 20.6$ mag, and $K_s = 19.7$ mag in tile LMC 6_4 and for $Y = 21.2$ mag, $J = 20.9$ mag, and $K_s = 19.9$ mag in tile LMC 6_6. The 50 per cent completeness level is reached at $Y = 19.9$ mag, $J = 19.5$ mag, and $K_s = 19.6$ mag in tile LMC 6_4 and at $Y = 20.4$ mag, $J = 20.1$ mag, and $K_s = 19.9$ mag in tile LMC 6_6, throughout the entire tile areas. Photometric completeness is used here as a reference to our knowledge of the faintest cluster MSTO reachable by our photometry.

3 THE CLUSTER SAMPLE

Recognizing catalogued star clusters in deep VMC tile images is neither straightforward nor simple. The catalogued objects were originally identified from optical images (e.g. from Digitized Sky Survey images; DSS[3]) which sometimes look rather different compared with their appearance at near-infrared wavelengths (bright red stars may dominate the cluster light while faint blue stars may be entirely absent in the near-infrared). In addition, the spatial resolution and depth of the images on which the clusters were identified differ from the equivalent parameters pertaining to the VMC images. Thus, for instance, single relatively bright stars might look like an unresolved compact cluster in images of lower spatial resolution, or unresolved background galaxies could be mistaken for small star clusters in shallower images. Offsets in the compiled coordinates with respect to the objects' centres cannot be ruled out either.

To avoid mismatches between observed objects and the actual list of catalogued clusters, we first overplotted the positions of the catalogued clusters on the deepest stacked K_s image. This way, based on using the coordinates resolved by the SIMBAD[4] astronomical data base, we unambiguously recognized the observed clusters one by one in the K_s image. Note that the main aim of this task is to confirm the compiled cluster coordinates and sizes so as to extract from the VMC photometric catalogues the magnitudes of the stars in the cluster region. We are not interested in properties such as the clusters' structures, stellar density profiles or radii, but we aim at obtaining accurate photometry for those stars which allow us to meaningfully define the clusters' fiducial sequences in their CMDs.

In order to build a cluster catalogue that is as complete as possible, we made use of those previously compiled by Pietrzyński & Udalski (2000, hereafter PU00), Bica et al. (2008, hereafter B08) and Glatt, Grebel & Koch (2010, hereafter G10). Particularly, B08 provided angular dimensions, which we used for assessing whether such regions contain sufficient numbers of stars to construct reliable cluster CMDs with the smallest fraction of unavoidable field-star contamination. While recognizing the catalogued clusters on the K_s tile image, we discarded those in the line of sight of H II regions, unresolved clusters, those for which the VMC photometry does not reach the MSTO or where the observed cluster CMDs do not show any cluster sequences. While attempting to cross-correlate the cluster names and their coordinates, we could not identify BSDL 1161 in the K_s tile image, and we found that SL 368 is listed at incorrect coordinates in B08 (and, hence, in SIMBAD as well). Nevertheless, G10 compiled the correct cluster loci. Our final cluster sample includes 313 catalogued clusters.

4 STAR CLUSTER PARAMETERS

In general terms, the observed CMDs of the selected objects are the result of the superposition of different stellar populations distributed along the line of sight. For this reason, using the observed CMDs without subtracting the luminosity function and colour distribution of field stars may lead to incorrect interpretations. Moreover, since the catalogued clusters were initially identified as small concentrations of stars on the basis of stellar density fluctuations, their real physical nature requires subsequent confirmation. In order to disentangle cluster stars from field stars, we used CMDs of adjacent fields to subtract the local LMC field luminosity function and colour distribution.

We constructed cluster CMDs based on all measured stars distributed within a circle with a radius of three times that tabulated by B08 based on visual inspection of the objects on DSS images or

[1] http://horus.roe.ac.uk/vsa/
[2] http://www.eso.org/sci/observing/phase3/data_releases.html
[3] The DSSs were produced at the Space Telescope Science Institute under US Government grant NAG W-2166. The images of these surveys are based on photographic data obtained using the Oschin Schmidt Telescope on Palomar Mountain and the UK Schmidt Telescope. The plates were processed into the present, compressed digital form with the permission of these institutions.
[4] http://simbad.u-strasbg.fr/simbad/

Downloaded from https://academic.oup.com/mnras/article-abstract/454/1/839/1143215 by guest on 24 April 2020

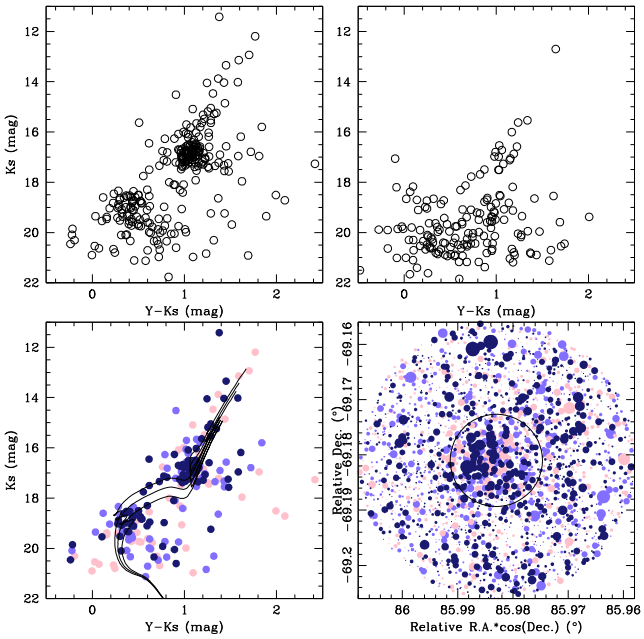


Figure 2. CMDs for stars in the field of NGC 2108: the observed CMD composed of the stars distributed within the cluster radius (top-left panel); a field CMD for an annulus – outer and inner radii equal to 3.163 and 3.0 times the cluster radius – centred on the cluster (top-right panel); the cleaned cluster CMD (bottom-left). Colour-scaled symbols represent stars that statistically belong to the field ($P \leq 25$ per cent, pink), stars that might belong to either the field or the cluster ($P = 50$ per cent, light blue), and stars that predominantly populate the cluster region ($P \geq 75$ per cent, dark blue). Three isochrones from Bressan et al. (2012) for $\log(t\ \mathrm{yr}^{-1}) = 8.8$, 8.9, and 9.0 and $Z = 0.006$ are also superimposed. The lack of fainter main-sequence stars results in less satisfactory matching at fainter magnitudes. The schematic diagram centred on the cluster for a circle of radius three times the cluster radius is shown in the bottom-right panel. The black circle represents the adopted cluster radius. Symbols are as in the bottom-left panel, with sizes proportional to the stellar brightnesses. North is up; east is to the left.

by us from the deepest K_s images. The objects are of small angular size, typically ∼0.6 arcmin (∼8.7 pc) in diameter. These regions are sufficiently large to encompass most of the cluster regions. Note that our main aim here is to clean the cluster CMDs from contamination by field stars within an area around the clusters' centres that is nine times larger than $\pi r^2_{\mathrm{cluster}}$, so that we do not need to trace their radial profiles. Once the cluster areas were delineated, we defined four additional regions with areas equal to the cluster regions and located more or less equidistant from the clusters' centres. For each of the latter regions, we constructed CMDs showing the defining features of the local LMC star field in that particular direction.

We next applied a procedure which was designed to compare each of the field CMDs to the cluster CMD and subtracted from the latter a representative field CMD in terms of stellar density, luminosity function, and colour distribution. This was done by comparing the numbers of stars counted in boxes distributed in a similar manner throughout all CMDs. The boxes were allowed to vary in size and position throughout the CMDs in order to meaningfully represent the actual distribution of field stars. For additional details, see Piatti et al. (2014, 2015), who applied this same procedure to other VMC data sets. Fig. 2 illustrates the performance of the cleaning procedure for NGC 2108, where we plotted three different CMDs: that for the stars located within the cluster radius (top-left panel), a single-field CMD for an annulus – outer and inner radii equal to 3.163 and 3.0 times the cluster radius – centred on the cluster, as well as the cleaned cluster CMD (bottom-left panel). The schematic diagram with a superimposed circle of radius equal to the cluster radius is shown in the bottom-right panel. The pink, light and dark blue filled circles in the bottom panels represent stars with cluster membership probabilities $P \leq 25$ per cent, $P = 50$ per cent, and $P \geq 75$ per cent, respectively. The 313 individual photometric catalogues for the studied clusters are provided in the online version of the journal. The columns of each catalogue successively lists the magnitude, the error and the sharpness for every source within a circle of radius three times that of the cluster and centred on the cluster's centre, in Y, J, and K_s, respectively, the RA and Dec. and the photometric membership probability (P). The latter is encoded with numbers 1, 2, 3, and 4 to represent probabilities of 25, 50, 75, and 100 per cent, respectively.

Table 1. Fundamental parameters of the LMC clusters studied here. We assume a distance modulus of 18.49 mag and a metallicity of [Fe/H] = −0.4 dex. The complete table is available online as Supporting Information.

Name	RA (°)	Dec. (°)	d (arcmin)	$E(B-V)$ (mag)	$\log(t\ \mathrm{yr}^{-1})$
–	–	–	–	–	–
NGC 1858	77.500	−68.904	0.70	0.30	7.30
HS 335	82.737	−69.341	0.40	0.10	8.60
NGC 2009	82.750	−69.182	0.80	0.15	7.50
–	–	–	–	–	–

We estimated reddening values and ages for our 313 sample clusters using the theoretical isochrones of Bressan et al. (2012) in the Vegamag system (where, by definition, Vega has a magnitude of zero in all filters), corrected by −0.074 mag in Y and −0.003 mag in K_s to put them on the VMC system (Rubele et al. 2015), to match the cleaned cluster CMDs. We adopted the same distance modulus for all clusters $(m - M)_0 = 18.49 \pm 0.09$ mag (de Grijs, Wicker & Bono 2014) and $K_s - M_{K_s} = (m - M)_0 + 0.372\ E(B - V)$, for $R_V = 3.1$ (Cardelli, Clayton & Mathis 1989; Gao et al. 2013), since by considering an average depth for the LMC disc of (3.44±1.16) kpc (Subramanian & Subramaniam 2009), we derived a smaller age difference than that resulting from the isochrones (characterized by the same metallicity) bracketing the observed cluster features in the CMD.

We used isochrones for $Z = 0.006$ ([Fe/H] = −0.4 dex), which corresponds to the mean LMC cluster metal content for the last ∼2–3 Gyr (Piatti & Geisler 2013). Additionally, the $Y - K_s$ colour is not sensitive to metallicity differences smaller than Δ[Fe/H] ∼0.4 dex, which is adequate given the spread of the stars in the CMDs (see Piatti et al. 2015). Indeed, we tried using isochrones with metallicities [Fe/H] = 0.0 dex and [Fe/H] = −0.7 dex and found negligible differences with respect to that of [Fe/H] = −0.4 dex, keeping in mind the relatively sparse nature of the majority of our clusters and the intrinsic spread of the stars in the CMDs. We found that isochrones bracketing the derived mean age by $\Delta E(B - V) = \pm 0.05$ mag and $\Delta\log(t\ \mathrm{yr}^{-1}) = \pm 0.1$ represent the overall uncertainties associated with the observed dispersion in the cluster CMDs. Although the dispersion is smaller in some cases, we prefer to retain the former values as an upper limit to our error budget. Table 1 lists the diameters used and the resulting reddening and age values obtained for the entire cluster sample, while the bottom-left panel of Fig. 2 illustrates the results of the isochrone matching for NGC 2108.

The resulting reddening distributions for the clusters located in tiles LMC 6_4 and 6_6 are shown in Fig. 3, where we have also

Downloaded from https://academic.oup.com/mnras/article-abstract/454/1/839/1143215 by guest on 24 April 2020

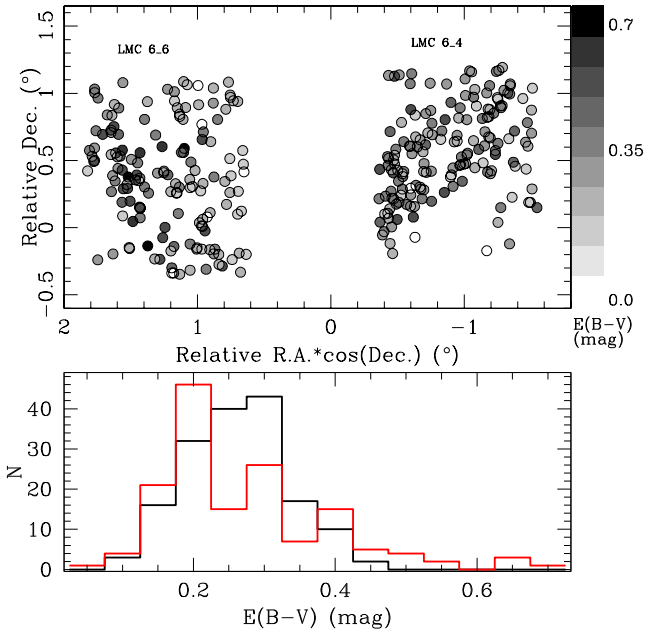


Figure 3. Reddening histograms for tiles LMC 6_4 (black) and LMC 6_6 (red; bottom panel) and the spatial distribution of the clusters' reddening, with darker shading representing higher reddening values (top panel). The grey-scale is in units of $E(B-V)$ (mag).

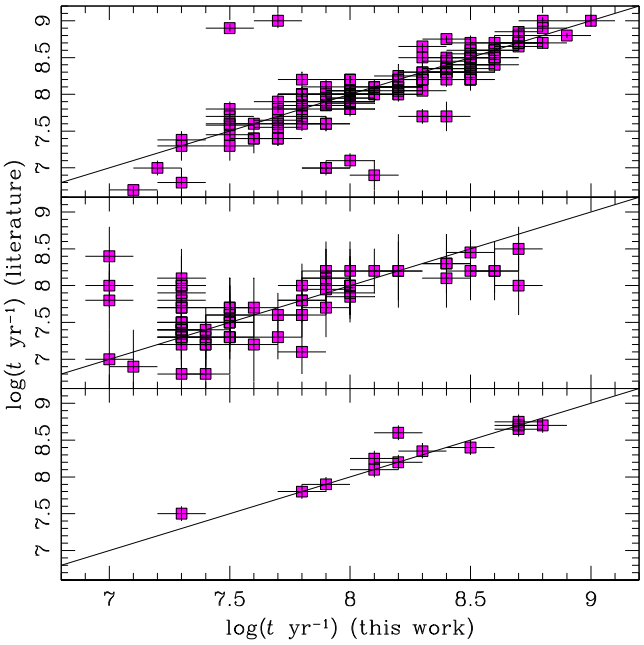


Figure 4. Comparison of the cluster age estimates derived here with those from the literature: PU00 (top panel), G10 (middle panel) and Washington photometry (Piatti 2012, 2014b; Choudhury, Subramaniam & Piatti 2015, bottom panel). Error bars and the locus of equality are also shown.

included an inset showing their spatial distribution. We converted $E(Y-K_s)$ to $E(B-V)$ using $E(Y-K_s) = 0.84E(B-V)$ (Cardelli et al. 1989). Both surveyed regions are characterized by a mean reddening spanning the range $E(B-V) \in [0.2, 0.3]$ mag. The tile centred on the LMC bar contains a slightly larger number of clusters with reddening values towards the upper limit of this range. On the other hand, the tile covering 30 Doradus includes clusters with reddening values in excess of $E(B-V) = 0.4$ mag. Bearing in mind that the observed cluster sequences are affected by interstellar extinction which is the sum of Milky Way (foreground) and LMC (internal) reddening, and that the mean Galactic reddening towards the LMC is $E(B-V) \approx 0.08$ mag (Dolphin et al. 2001; Schlafly & Finkbeiner 2011), it follows that the average (internal) reddening in these particular LMC regions is ∼0.1–0.2 mag. This range is in very good agreement with a number of previous estimates (e.g. Oestreicher, Gochermann & Schmidt-Kaler 1995; Subramanian & Subramaniam 2009; Tatton et al. 2013), although slightly lower values have also been found from analysis of field red-clump and variable stars (Clementini et al. 2003; Haschke, Grebel & Duffau 2011).

Fig. 4 shows a comparison of the cluster age estimates derived here with those previously obtained from similar isochrone matching. The latter assumed a constant metal content for the LMC of [Fe/H] = −0.4 dex, a distance modulus of 18.50 mag (except PU00 who adopted 18.24 mag and mentioned that change in the distance modulus by about 0.15 mag produced difference in ages of less than a few per cent, which is much less than the derived errors), and isochrones computed by the Padova group (Bertelli et al. 1994; Marigo et al. 2008). Agreement with the OGLE-based age estimates (200 clusters) is good, just like that with the cluster ages determined on the basis of Washington photometry (Piatti 2012, 2014b; Choudhury et al. 2015, 3, 7 and 3 clusters, respectively). The most discrepant points in the OGLE age comparison are associated with clusters whose CMDs include relatively bright blue stars that PU00 either rejected or included in the isochrone matching, thus resulting in, respectively, older (HS 223, $\log(t\ \mathrm{yr}^{-1}) = 8.9$; BSDL 725, $\log(t\ \mathrm{yr}^{-1}) = 9.0$) or younger (HS 362, $\log(t\ \mathrm{yr}^{-1}) = 6.9$; HS 219, and $\log(t\ \mathrm{yr}^{-1}) = 7.0$; H 88-169, $\log(t\ \mathrm{yr}^{-1}) = 7.1$) ages than our values. As for the comparison with the ages based on Washington photometry, which were obtained from isochrone matching to CMDs previously corrected for field-star contamination using the same technique described above and for clusters not studied by either PU00 or G10, better agreement can still be achieved. The correlation with the ages determined by G10 (89 clusters) is less tight, because G10 did not perform field-star decontamination, although these authors mention that field contamination is a severe effect in the extracted cluster CMDs and may, therefore, affect the age estimates significantly. Consequently, their age estimates likely reflect the composite LMC stellar populations [e.g. KMK 88-74 ($\log(t\ \mathrm{yr}^{-1}) = 7.8$), BSDL 2807, ($\log(t\ \mathrm{yr}^{-1}) = 8.0$), KMK 88-86 ($\log(t\ \mathrm{yr}^{-1}) = 8.4$)]. This possibility alerts us to the fact that solely the circular extraction of the observed CMDs of clusters located in highly populated stellar fields is not sufficient for accurate isochrone matching of the main cluster features (see also Piatti & Bica 2012; Piatti 2014b; Piatti et al. 2014, 2015).

Based on Fig. 4, we conclude that the age scale derived in this paper is consistent with those pertaining to our comparison samples. We can therefore safely merge these samples to compile a larger cluster sample characterized by an age distribution put on an homogeneous scale. Of our 313 sample clusters, 95 did not have any previous age estimates – a ∼30 per cent increase of clusters with known ages in these fields. The final cluster age catalogue is composed of our 313 age estimates, combined with 74 clusters from PU00, five clusters from G10 and 15 clusters from other studies (mainly based on Washington photometry). Whenever a cluster has more than one age estimate, we adopted a weighed average value. All ages considered here were derived based on isochrone matching of the cluster CMDs, spanning the age range $7.0 < (\log(t\ \mathrm{yr}^{-1}) < 9.0$. Fig. 5 shows the clusters' spatial distribution,

Downloaded from https://academic.oup.com/mnras/article-abstract/454/1/839/1143215 by guest on 24 April 2020

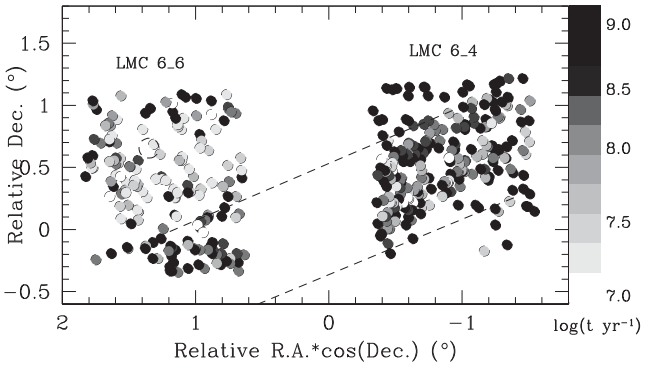


Figure 5. Spatial distribution of the cluster ages, with darker shading representing older ages, centred at RA = $05^h23^m34^s$, Dec. = $-69°45'22''$(J2000). North is up; east is to the left. The grey-scale is in units of log (t yr^{-1}). The locations of 30 Doradus and the LMC bar are indicated with a dashed circle and two parallel lines (Subramaniam & Subramanian 2009), respectively.

with darker points representing older ages. Note the obvious distribution of very young clusters around 30 Doradus in tile LMC 6_6, as well as of young clusters in the innermost regions of the bar in tile LMC 6_4.

5 THE CFs IN TILES LMC 6_4 AND 6_6

A number of different studies have shown that the LMC's field SFR is variable across the galaxy (Rubele et al. 2012; Meschin et al. 2014; Harris & Zaritsky 2009, hereafter HZ09). In particular, HZ09 concluded from the concordance between the star formation and chemical-enrichment histories of the field and cluster populations that the field and cluster star formation modes are tightly coupled. Recently, Piatti & Geisler (2013) studied 21 LMC regions spread across the main body of the galaxy and found that the cluster and field star age–metallicity relationships (AMRs) of such regions show a satisfactory match only for the last 3 Gyr, i.e. log (t yr^{-1}) $\leq$ 9.5, while for the oldest ages – t > 11 Gyr, log (t yr^{-1}) > 10.05 – the cluster AMR represents a lower envelope to the field AMR.

We are interested in constructing the CFs, i.e. the number of clusters formed per unit time interval as a function of age, as a function of position in both tiles studied here. It would appear reasonable to infer that if the star formation history of LMC field stars has been different throughout the galaxy, and field stars and clusters show some evidence of common formation and chemical-enrichment histories, then the CFs should reflect the same spatial variations as seen in the field stars. Piatti (2014a, hereafter P14) showed that the number of catalogued clusters without age estimates is relatively small with respect to the total number of catalogued clusters in the LMC. He also showed that nearly half of the more massive clusters in his sample with age estimates mostly trace the overall behaviour of the CFs. Alternatively, clusters with masses below 10^3 M$_\odot$ for ages younger than 1 Gyr do not contribute significantly to the normalized CFs, although they represent on average nearly half of the total number of clusters with age estimates. In addition, he found that different model age distributions for the total number of clusters without age estimates do not affect the resulting CFs. Moreover, he concluded that possible incompleteness of non-catalogued clusters (which include the faintest clusters in the galaxy) does not play an important role in the resulting CFs either. Since our cluster age catalogue for the two LMC tiles of interest contains ∼30 per cent more clusters than previously known, we are confident that we can consider our results statistically robust. Indeed, our cluster sample includes ∼80 per cent of the catalogued clusters in the surveyed regions.

In constructing the CFs, we first divided the tiles into 12 subregions of similar size, and then counted the number of clusters in each region, taking into account bin size and age uncertainty effects. This procedure allowed us to build age histograms (and hence CFs) which best reproduce the intrinsic age distribution of each subregion. For additional details about the treatment of bin size and age uncertainty effects, see, e.g. Piatti & Geisler (2013), P14 and Piatti et al. (2015). All CFs were normalized to the total number of clusters included in our sample. We assume that there has been no statistically significant mixing of clusters for ages of log (t yr^{-1}) < 9.0 (which represents less than the last 10 per cent of the galaxy's lifetime) between regions. Indeed, van der Marel & Kallivayalil (2014) showed that for most tracers (including clusters and field stars), the LMC's line-of-sight velocity dispersion is at least a factor of ∼2 smaller than the corresponding rotation velocity, which implies that the LMC as a whole is a kinematically cold disc system. Figs 6 and 7 show the resulting CFs for the subregions of tiles LMC 6_4 and 6_6, respectively. We include insets with the schematic distribution of the 12 subregions and a colour reference of the respective CF curves. From Fig. 6, it is clear that the outermost subregions of the LMC bar, which crosses tile LMC 6_4 along the SE–NW diagonal (blue lines), have experienced more prominent cluster formation in the past – log (t yr^{-1}) ∼ 8.5–9.0 – and more recently, log (t yr^{-1}) < 7.7, cluster formation in the innermost regions has become more active (red and green lines). However, the cluster formation scenario in the central parts of the bar appears to be rather complex and patchy. In tile LMC 6_6 (Fig. 7), the most striking role is played by the 30 Doradus region, which dominates the recent cluster formation activity (dark green and black lines). Likewise, 30 Doradus is spatially surrounded by cluster formation activity characterized by older ages with increasing distance from the object (blue and red lines), possibly approaching the intrinsic CF in the outer LMC bar (see fig. 5 in P14).

We also compiled composite CFs using all clusters located within each tile and compared them with those previously obtained by P14 for HZ09's bar and the 30 Doradus region (see fig. 6 in HZ09). The CFs were constructed by taking into account bin sizes and age uncertainties, and normalized to the total number of clusters. Figs 8 and 9 show the resulting CFs and those from P14, represented by black and grey lines, respectively. Both pairs of CF curves are very similar. CF differences become important for log (t yr^{-1}) ∈ [7.2, 7.6]. These differences are likely owing to the fact that P14's CF covers the entire LMC bar, while the present CF targets its central part only, which is characterized by a relative excess of younger clusters with respect to the entire bar. On the other hand, the most noticeable differences between the CFs centred on 30 Doradus occur for older ages – log (t yr^{-1}) > 8.5 – which is most likely also caused by the larger area covered by HZ09 than our tile LMC 6_6, which thus implies that the HZ09 CF is composed of a relatively smaller fraction of older clusters. We superimposed on Figs 8 and 9 the CFs (red lines) and the corresponding uncertainties for the bar region in HZ09 as well as their 30 Doradus region, respectively, assuming that clusters are born according to a power-law mass distribution with a slope $\alpha = -2$ and at a rate that is proportional to the SFR determined by HZ09 for each region. The shapes of the CFs recovered from the SFR curves generally follow those of the observed CFs, although the cluster and field-star populations do not seem to have evolved as fully coupled systems. Nevertheless, coupling between

Downloaded from https://academic.oup.com/mnras/article-abstract/454/1/839/1143215 by guest on 24 April 2020

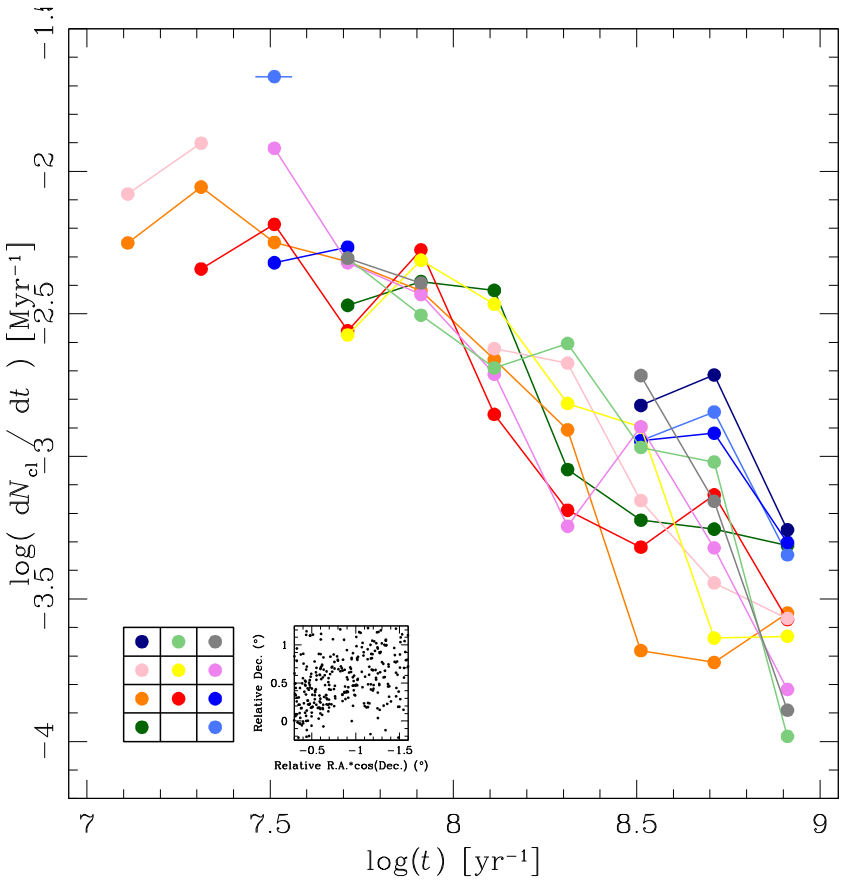


Figure 6. CFs for subregions in tile LMC 6_4. The bottom-right hand panel shows the spatial distribution of the Bica et al. (2008) catalogue of star clusters, while the left-hand panel schematically represents the subregions and indicates the colour used in drawing the respective CFs. North is up and east is to the left. Note that computed values (filled circles) for each CF are connected by a solid line. Some CFs do not have points for certain age intervals because of the lack of clusters within them, which resulted in truncated CFs. In such cases, we drew isolated points with a short line to represent that they belong to a truncated CF. One subregion does not contain any cluster in our sample.

field-star and cluster formation appears to have been dominant for both regions.

Assuming that most – if not all – stars form in clustered modes (Lada & Lada 2003), our results suggest that the combination of cluster formation and disruption rates (which depend on environmental conditions, cluster masses, among others) still provides a positive balance, in the sense that the cluster population has not been entirely transformed into field stars. Baumgardt et al. (2013) showed that about 90 per cent of all clusters older than 200 Myr are lost per dex of lifetime, which implies a cluster dissolution rate significantly faster than that based on analytic estimates and *N*-body simulations. However, de Grijs et al. (2013) showed that there is no evidence of significant destruction, other than that expected from stellar dynamics and evolution in simple population models for ages up to 1 Gyr ($\log(t\ \mathrm{yr}^{-1}) = 9$). As can be seen, the issue about at what pace cluster disruption takes place in different LMC regions and even whether field stars mostly come from cluster disruption still needs further study. Our results do not allow us to draw any further conclusion about this issue, but that the cluster formation has been different in the studied regions.

By comparing our results with those of HZ09 for the two tiles, some hint about the distinct roles played by the environments can be drawn, since differences in CF are larger in the tile LMC 6_6 than in LMC 6_4 for ages younger than $\log(t\ \mathrm{yr}^{-1}) < 8.0$. Werchan & Zaritsky (2011) tabulated the concentration, central surface brightness, tidal radii, 90 per cent enclosed luminosity radii, and local background luminosity density for 1066 star clusters in the Magellanic Cloud Phomotometric Survey (MCPS; Zaritsky et al. 2002). They found that while most of the star clusters are similar between the LMC and the SMC populations, the LMC lacks star clusters that are large, either in terms of core or 90 per cent enclosed luminosity radii as the largest in the SMC, and suggested that this result could be featuring a signature of larger tidal stresses in the LMC. On the other hand, Wilkinson et al. (2003) used *N*-body simulations of star clusters to investigate the possible dynamical origins of the observed spread in core radius among intermediate-age and old star clusters in the LMC and concluded that the tidal field of the LMC has not yet significantly influenced the evolution of the intermediate-age clusters. In this sense, we interpret that the actual dynamical state of the studied LMC clusters might be a combination of an age effect (two-body relaxation) and their locations in the galaxy (see e.g. Glatt et al. 2011, for the SMC).

Finally, we compared the CFs derived here with those obtained from the SFRs derived by Rubele et al. (2012) for tile LMC 6_6. The latter authors derived the SFRs for two subregions (D1 and D2; see their fig. 2). They used the 'partial model' technique, which applies a linear combination of partial models that optimally matches the observed Hess diagrams allowing the distance modulus, visual extinction, age, and metallicity to vary, convolved with the distributions of photometric errors and completeness. The coefficients of

Downloaded from https://academic.oup.com/mnras/article-abstract/454/1/839/1143215 by guest on 24 April 2020

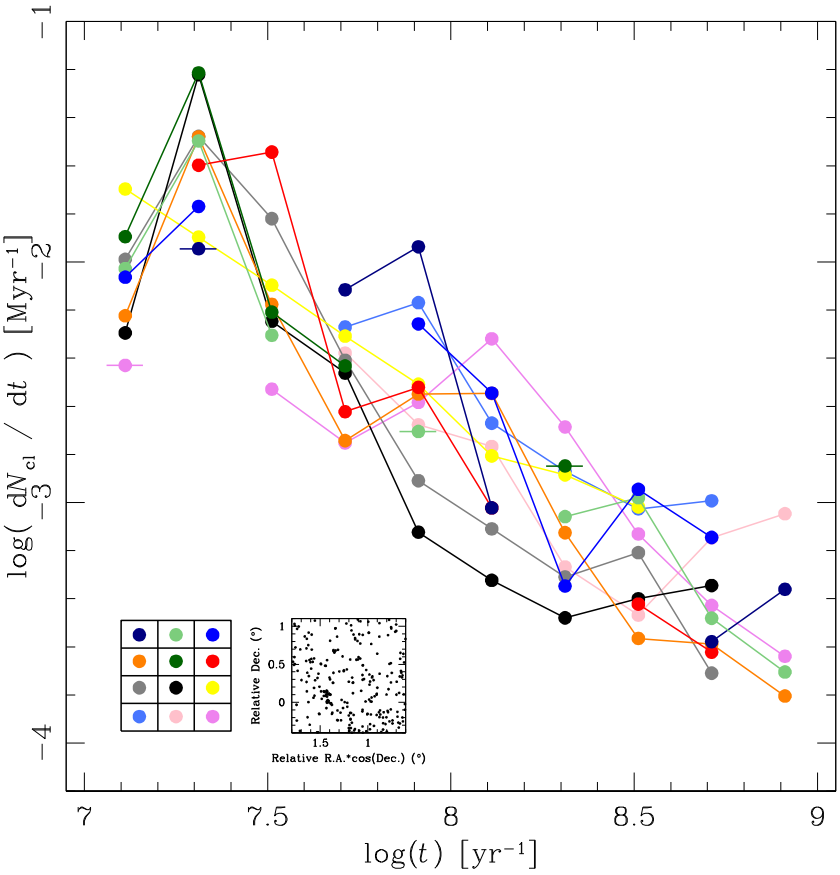


Figure 7. As Fig. 6, but for tile LMC 6_6.

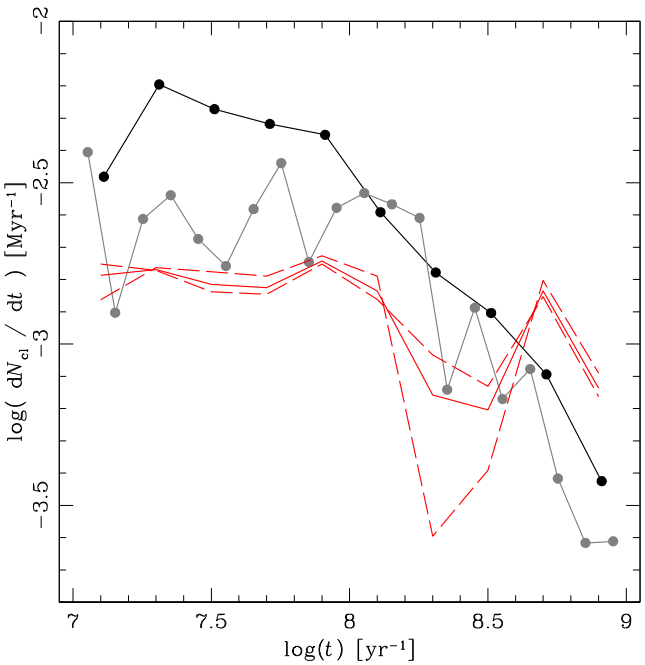


Figure 8. Composite CF for tile LMC 6_4 (black) compared with those obtained by P14 for clusters within HZ09's bar region (grey) and by HZ09 for the respective mean SFR and its 1σ uncertainty (solid and dashed red lines, respectively).

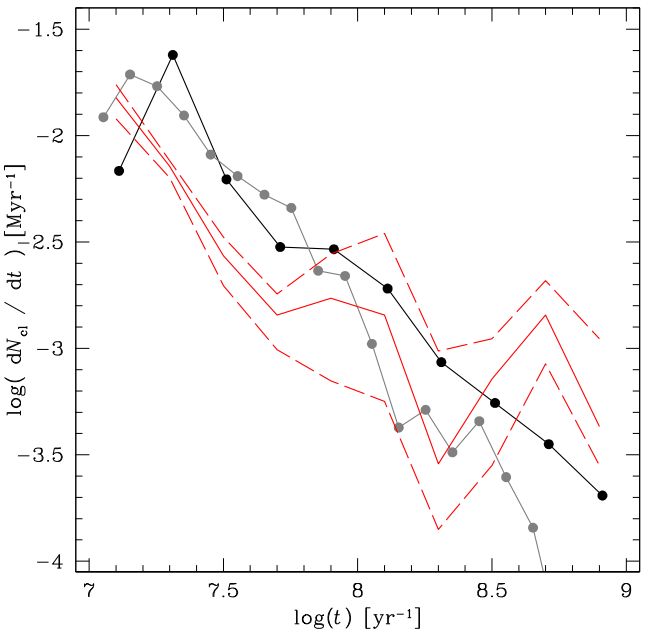


Figure 9. As Fig. 8, but for tile LMC 6_6 and HZ09's 30 Doradus region.

this linear combination of partial models (including the best-fitting distance modulus and extinction) are directly converted into the SFRs. We used their SFRs and cluster masses from $\log(M_{\rm cl}[{\rm M}_\odot]) = 2.2$ to $\log(M_{\rm cl}[{\rm M}_\odot]) = 5.0$ (de Grijs & Goodwin 2008; Glatt et al. 2011), and normalized the resulting CFs by the total number of

Downloaded from https://academic.oup.com/mnras/article-abstract/454/1/839/1143215 by guest on 24 April 2020

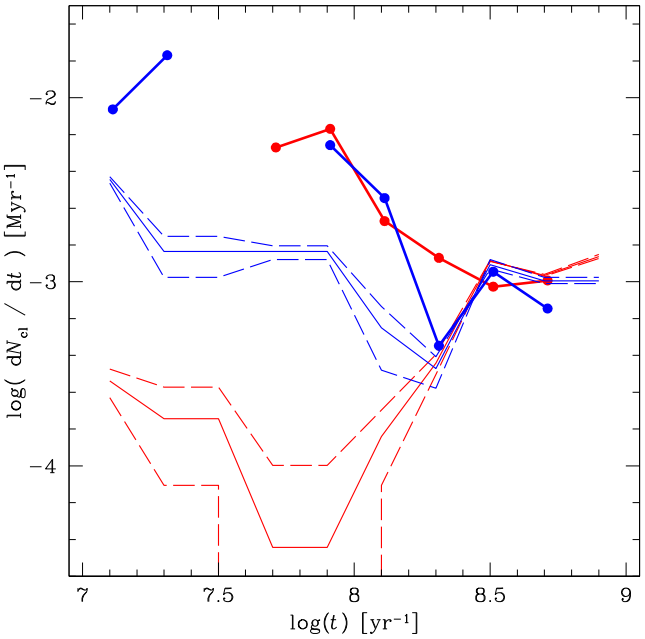


Figure 10. CFs for subregions D1 (thick red line) and D2 (thick blue line) in tile LMC 6_6. Thin and dashed lines represent, respectively, the mean CFs and their 1σ dispersions recovered from the corresponding SFRs obtained by Rubele et al. (2012).

clusters used, so that they can be compared directly with the observed distributions. Fig. 10 shows the resulting, recovered CFs, where the uncertainties are indicated by dashed lines. The observed and recovered CFs are clearly different for ages younger than $\log(t\,\mathrm{yr}^{-1}) \sim 8.0$. Even though the recovered CFs require additional refinements, the cluster excesses could be evidence of relatively recent enhanced cluster formation in this part of the galaxy. Likewise, note that both recovered CFs are different between them, which suggests either that cluster disruption changed dramatically from one subregion to the other, or field stars did not come from cluster disruption in a similar proportion. Rubele et al. (2012, 2015) showed that the SFR of field stars varies with the position in the LMC and SMC, respectively. Conversely, P14 and Piatti et al. (2015) found evidence that a similar behaviour occurs within the LMC and SMC cluster populations, but not with a completely equivalent pace to field stars. These results, besides those derived here, provide some clues for a better approach in the study of the field stars origin and its link to cluster disruption and environmental conditions.

6 CONCLUSIONS

In this paper, we have analysed CMDs of previously catalogued star clusters located in the innermost region of the LMC based on a YJK_s photometric data set obtained by the VMC collaboration. We focused on tiles LMC 6_4 (located in the central part of the LMC bar) and 6_6 (centred on 30 Doradus), because they are among the first fully completed tiles of the VMC survey, and they show the most recent star formation activity in the galaxy. We obtained PSF photometry for stars in and projected along the line of sight towards 313 catalogued clusters, which represents a statistically meaningful sample size.

We applied a field-star subtraction procedure to statistically clean the cluster CMDs from field-star contamination and to disentangle cluster features from those associated with their surrounding fields. The technique we employed makes use of variable cells to reproduce the field CMDs as closely as possible. Based on matching theoretical isochrones in the VISTA system to the cleaned cluster CMDs, we obtained estimates of the clusters' reddening values and ages, assuming a distance modulus of 18.49 mag and a metallicity of $Z = 0.006$ ([Fe/H] $= -0.4$ dex). Both surveyed regions are affected by a mean reddening spanning the range $E(B-V) \in [0.2, 0.3]$ mag; the average internal (LMC) reddening amounts to ∼0.1–0.2 mag. In addition, the tile covering 30 Doradus includes clusters with reddening values in excess of $E(B-V) = 0.4$ mag.

The resulting cluster ages span the age range $7.0 \leq \log(t\,\mathrm{yr}^{-1}) < 9.0$. They form part of the cluster data base which will result from the VMC survey and which will be used to self-consistently study the overall cluster formation history of the Magellanic system. The age scale derived in this paper is consistent with those resulting from previous publications, in particular those based on OGLE (Pietrzyński & Udalski 2000), the Magellanic Cloud Photometric Surveys (Zaritsky et al. 2002), and the Washington photometric system (Piatti 2012, 2014b; Choudhury et al. 2015), among others. A total of 95 clusters of the 313 objects in our sample had their ages determined for the first time. This represents an increase of ∼30 per cent of clusters with known ages in the two LMC tile regions. The enlarged catalogue of clusters with age estimates contains 407 objects.

Based on analysis of this statistically complete cluster sample, we addressed the nature of variations in the LMC CF in terms of the clusters' spatial distribution. Particular attention was paid to bin sizes and age uncertainties in constructing CFs for 12 different subregions of similar sizes, homogeneously distributed within each LMC tile. As for tile LMC 6_4, we found that the outermost subregions of the LMC bar experienced enhanced cluster formation activity in the past – $\log(t\,\mathrm{yr}^{-1}) \in [8.5, 9.0]$ – whereas more recently, $\log(t\,\mathrm{yr}^{-1}) < 7.7$, cluster formation seems to occur more frequently in the inner regions. Overall, however, cluster formation in the central parts of the bar has proceeded in a patchy manner. On the other hand, in tile LMC 6_6, the 30 Doradus subregions play the most striking role in the very recent cluster formation history. They are surrounded by successively older clusters for increasing distances from 30 Doradus.

Finally, we compared the composite CFs for each LMC tile to those recovered assuming that clusters have formation rates similar to the known field SFRs. The shapes of the recovered CFs, and more particularly those for the subregions near 30 Doradus, suggest that cluster and field-star populations do not seem to have evolved as fully coupled systems during the last ∼100 Myr. The cluster excesses found could be evidence of relatively recent enhanced cluster formation in these parts of the galaxy and thus confirm both that most stars are formed in clusters and that there is no significant destruction other than that expected from stellar dynamics and evolution of simple stellar population models for ages up to 1 Gyr.

ACKNOWLEDGEMENTS

We thank the Cambridge Astronomy Survey Unit (CASU) and the Wide-Field Astronomy Unit (WFAU) in Edinburgh for providing calibrated data products under the support of the Science and Technology Facilities Council (STFC) in the UK. This research has made use of the SIMBAD data base, operated at CDS, Strasbourg, France. This study is based on observations obtained with VISTA at the Paranal Observatory under programme ID 179.B-2003. We thank the anonymous referee whose comments and suggestions helped us to improve the manuscript. RG acknowledges research

Downloaded from https://academic.oup.com/mnras/article-abstract/454/1/839/1143215 by guest on 24 April 2020

support from the National Natural Science Foundation of China (NSFC; grant 11373010).

REFERENCES

Anders P., de Grijs R., Fritze-v. Alvensleben U., Bissantz N., 2004, MNRAS, 347, 17
Ashman K. M., Zepf S. E., 1992, ApJ, 384, 50
Bagheri G., Cioni M.-R. L., Napiwotzki R., 2013, A&A, 551, A78
Barker S., de Grijs R., Cerviño M., 2008, A&A, 484, 711
Bastian N., Gieles M., Lamers H. J. G. L. M., Scheepmaker R. A., de Grijs R., 2005, A&A, 431, 905
Baumgardt H., Parmentier G., Anders P., Grebel E. K., 2013, MNRAS, 430, 676
Bertelli G., Bressan A., Chiosi C., Fagotto F., Nasi E., 1994, A&AS, 106, 275
Bertin E., Mellier Y., Radovich M., Missonnier G., Didelon P., Morin B., 2002, in Bohlender D. A., Durand D., Handley T. H., eds, ASP Conf. Ser. Vol. 281, Astronomical Data Analysis Software and Systems XI. Astron. Soc. Pac., San Francisco, p. 228
Bica E., Bonatto C., Dutra C. M., Santos J. F. C., 2008, MNRAS, 389, 678 (B08)
Bressan A., Marigo P., Girardi L., Salasnich B., Dal Cero C., Rubele S., Nanni A., 2012, MNRAS, 427, 127
Cardelli J. A., Clayton G. C., Mathis J. S., 1989, ApJ, 345, 245
Cezario E., Coelho P. R. T., Alves-Brito A., Forbes D. A., Brodie J. P., 2013, A&A, 549, A60
Choudhury S., Subramaniam A., Piatti A. E., 2015, AJ, 149, 52
Cioni M.-R. L. et al., 2011, A&A, 527, A116
Clementini G., Gratton R., Bragaglia A., Carretta E., Di Fabrizio L., Maio M., 2003, AJ, 125, 1309
Colucci J. E., Bernstein R. A., 2012, ApJ, 749, 124
de Grijs R., 2010, Phil. Trans. R. Soc. A, 368, 693
de Grijs R., Anders P., 2006, MNRAS, 366, 295
de Grijs R., Goodwin S. P., 2008, MNRAS, 383, 1000
de Grijs R., Parmentier G., 2007, Chin. J. Astron. Astrophys., 7, 155
de Grijs R., O'Connell R. W., Gallagher J. S., III, 2001, AJ, 121, 768
de Grijs R., Goodwin S. P., Anders P., 2013, MNRAS, 436, 136
de Grijs R., Wicker J. E., Bono G., 2014, AJ, 147, 122
de Meulenaer P., Narbutis D., Mineikis T., Vansevičius V., 2013, A&A, 550, A20
Dolphin A. E., Walker A. R., Hodge P. W., Mateo M., Olszewski E. W., Schommer R. A., Suntzeff N. B., 2001, ApJ, 562, 303
Elmegreen B. G., Efremov Y. N., 1997, ApJ, 480, 235
Emerson J. P., Sutherland W. J., 2010, in Stepp L. M., Gilmozzi R., Hall H. J., eds, Proc. SPIE Conf. Ser. Vol. 7733, Ground-based and Airborne Telescopes III. SPIE, Bellingham, p. 773306
Emerson J. P. et al., 2004, in Quinn P. J., Bridger A., eds, Proc. SPIE Conf. Ser. Vol. 5493, Optimizing Scientific Return for Astronomy through Information Technologies. SPIE, Bellingham, p. 401
Emerson J., McPherson A., Sutherland W., 2006, The Messenger, 126, 41
Fall S. M., 2006, ApJ, 652, 1129
Fall S. M., Chandar R., Whitmore B. C., 2005, ApJ, 631, L133
Gao J., Jiang B. W., Li A., Xue M. Y., 2013, ApJ, 776, 7
Geha M. C. et al., 1998, AJ, 115, 1045
Gieles M., Lamers H. J. G. L. M., Portegies Zwart S. F., 2007, ApJ, 668, 268
Glatt K., Grebel E. K., Koch A., 2010, A&A, 517, A50 (G10)
Glatt K. et al., 2011, AJ, 142, 36
Goodwin S. P., Bastian N., 2006, MNRAS, 373, 752
Hambly N. C., Mann R. G., Bond I., Sutorius E., Read M., Williams P., Lawrence A., Emerson J. P., 2004, in Quinn P. J., Bridger A., eds, Proc. SPIE Conf. Ser. Vol. 5493, Optimizing Scientific Return for Astronomy through Information Technologies. SPIE, Bellingham, p. 423
Harris J., Zaritsky D., 2009, AJ, 138, 1243 (HZ09)
Haschke R., Grebel E. K., Duffau S., 2011, AJ, 141, 158
Irwin M. J. et al., 2004, in Quinn P. J., Bridger A., eds, Proc. SPIE Conf. Ser. Vol. 5493, Optimizing Scientific Return for Astronomy through Information Technologies. SPIE, Bellingham, p. 411
Lada C. J., Lada E. A., 1991, in Janes K., ed., ASP Conf. Ser. Vol. 13, The Formation and Evolution of Star Clusters. Astron. Soc. Pac., San Francisco, p. 3
Lada C. J., Lada E. A., 2003, ARA&A, 41, 57
Marigo P., Girardi L., Bressan A., Groenewegen M. A. T., Silva L., Granato G. L., 2008, A&A, 482, 883
Mengel S., Lehnert M. D., Thatte N., Genzel R., 2005, A&A, 443, 41
Meschin I., Gallart C., Aparicio A., Hidalgo S. L., Monelli M., Stetson P. B., Carrera R., 2014, MNRAS, 438, 1067
Oestreicher M. O., Gochermann J., Schmidt-Kaler T., 1995, A&AS, 112, 495
Olszewski E. W., Suntzeff N. B., Mateo M., 1996, ARA&A, 34, 511
Parmentier G., de Grijs R., 2008, MNRAS, 383, 1103
Piatti A. E., 2012, A&A, 540, A58
Piatti A. E., 2014a, MNRAS, 437, 1646 (P14)
Piatti A. E., 2014b, MNRAS, 440, 3091
Piatti A. E., Bica E., 2012, MNRAS, 425, 3085
Piatti A. E., Geisler D., 2013, AJ, 145, 17
Piatti A. E. et al., 2014, A&A, 570, A74
Piatti A. E., de Grijs R., Rubele S., Cioni M.-R. L., Ripepi V., Kerber L., 2015, MNRAS, 450, 552
Pietrzyński G., Udalski A., 2000, Acta Astron., 50, 337 (PU00)
Rubele S. et al., 2012, A&A, 537, A106
Rubele S. et al., 2015, MNRAS, 449, 639
Sarajedini A., 1998, AJ, 116, 738
Schlafly E. F., Finkbeiner D. P., 2011, ApJ, 737, 103
Stetson P. B., Davis L. E., Crabtree D. R., 1990, in Jacoby G. H., ed., ASP Conf. Ser. Vol. 8, CCDs in Astronomy. Astron. Soc. Pac., San Francisco, p. 289
Subramaniam A., Subramanian S., 2009, ApJ, 703, L37
Subramanian S., Subramaniam A., 2009, A&A, 496, 399
Tatton B. L. et al., 2013, A&A, 554, A33
van der Marel R. P., Kallivayalil N., 2014, ApJ, 781, 121
Werchan F., Zaritsky D., 2011, AJ, 142, 48
Whitmore B. C., 2004, in Lamers H. J. G. L. M., Smith L. J., Nota A., eds, ASP Conf. Ser. Vol. 322, The Formation and Evolution of Massive Young Star Clusters. Astron. Soc. Pac., San Francisco, p. 419
Whitmore B. C., Chandar R., Fall S. M., 2007, AJ, 133, 1067
Wilkinson M. I., Hurley J. R., Mackey A. D., Gilmore G. F., Tout C. A., 2003, MNRAS, 343, 1025
Zaritsky D., Harris J., Thompson I. B., Grebel E. K., Massey P., 2002, AJ, 123, 855

SUPPORTING INFORMATION

Additional Supporting Information may be found in the online version of this article:

Table 1. Fundamental parameters of the LMC clusters studied here.
Clusters.sub.tar
(http://www.mnras.oxfordjournals.org/lookup/suppl/doi:10.1093/mnras/stv2054/-/DC1).

Please note: Oxford University Press are not responsible for the content or functionality of any supporting materials supplied by the authors. Any queries (other than missing material) should be directed to the corresponding author for the article.

This paper has been typeset from a TEX/LATEX file prepared by the author.

Downloaded from https://academic.oup.com/mnras/article-abstract/454/1/839/1143215 by guest on 24 April 2020